Only male fin whales sing loud songs

These mammals need to call long-distance when it comes to attracting females.

The low-frequency vocalizations of fin and blue whales are the most powerful and ubiquitous biological sounds in the ocean[1,2]. Here we combine acoustic localization and molecular techniques to show that, in fin whales, only males produce these vocalizations. This finding indicates that they may function as male breeding displays, and will help to focus concern on the impact of human-generated low-frequency sounds on recovering whale populations.

The long, patterned 15–30-Hz ('20-Hz') vocal sequences of fin whales (*Balaenoptera physalus*) can reach intensities of 184–186 decibels (dB) relative to 1 μPa of sound pressure, and can be detected throughout the world's oceans[3,4]. However, the source of these vocalizations was hard to identify[5] because of the inherent difficulty of studying wide-ranging pelagic species and in locating low-frequency sound sources in the ocean. Until now, their function was therefore unknown[6], making it difficult to assess the effects of increasing levels of human-produced sounds on these whales[7].

We investigated whether these vocalizations could be breeding displays[8] by determining the sex of vocalizing fin whales (Fig. 1) and comparing the results to the overall sex ratio in Loreto Bay, Gulf of California, Mexico. We identified and tracked vocalizing fin whales by using a 120-metre-long towed array of hydrophones and beam-forming software to compute a series of cross-bearings to a vocalizing individual. Required confirmation criteria included the absence of other whales that could potentially match the acoustic cross-bearings, and asynchronization of vocalizations with respiration.

Once the vocalizing animal was unambiguously identified, a skiff was deployed to obtain a biopsy sample in order to ascertain its sex[9]. To estimate the overall sex ratio in the study area, we took biopsy samples from all fin whales encountered during systematic weekly surveys.

Vocalizations were produced only by male fin whales, despite a 1:1 overall sex ratio in the area (vocalizing: males, 9; females, 0; binomial test, $P < 0.001$; population: males, 21; females, 22; binomial test with normal approximation, $Z_{0.05,2} = 0.153$, $P = 0.879$). This sexual dichotomy in vocal behaviour supports the idea that the patterned sounds of fin whales are male breeding displays.

We propose that these displays serve to attract females from great distances to aggregations of patchily distributed prey. This is supported by several observations.

B. R. TERSHY

Figure 1 Only boys make noise: the wide dispersal of populations of the fin whale, seen here surfacing off the Mexican coast, means that males have to sing extra loudly to woo females.

First, fin and blue whales (*Balaenoptera musculus*) do not aggregate in specific areas for breeding, a behavioural trait that distinguishes them from the closely related humpback whale (*Megaptera novaeangliae*)[10]. Second, we previously found that fin whales use the Loreto study area to forage on dense aggregations of krill[11]. Third, the low-frequency vocalizations of *Balaenoptera* spp. are optimal for long-distance communication in deep water[12].

Our results help to focus growing concern over the effects of human-produced sound on *Balaenoptera* spp.[13]. Sound levels from commercial ships, military sonar, seismic surveys and ocean acoustic research are extremely high (190–250 dB relative to 1 μPa at 1 m; ref. 4) and, at least since the early 1960s, the amount of human-produced sound in the frequency range used by large whales has increased[7]. A sound is detectable if its received level exceeds that of background noise by enough to be detected by the animal. An increase in ambient noise could thus reduce the distance over which receptive females might hear the vocalizations of males. To the extent that growth of *Balaenoptera* populations is limited by the encounter rate of receptive females with singing males, the recovery of fin- and blue-whale populations from past exploitation could be impeded by low-frequency sounds generated by human activity.

Donald A. Croll*, Christopher W. Clark†, Alejandro Acevedo‡, Bernie Tershy*, Sergio Flores§, Jason Gedamke*, Jorge Urban§

**Department of Ecology and Evolutionary Biology, Center for Ocean Health, University of California, Santa Cruz, California 95060, USA*
e-mail: croll@biology.ucsc.edu
†Cornell Laboratory of Ornithology, Bioacoustics Research Program, 159 Sapsucker Woods Road, Ithaca, New York 14850, USA
‡California Academy of Sciences, 55 Concourse Drive, Golden Gate Park, San Francisco, California 94118, USA
§Universidad Autónoma de Baja California Sur, AP 19-B, La Paz, BCS 23080, Mexico

1. Aroyan, J. L. *et al.* in *Hearing by Whales and Dolphins* (eds Au, W. W. L., Popper, A. N. & Fay, R. N.) 409–469 (Springer, New York, 2000).
2. Thode, A. M., D'Spain, G. L. & Kuperman, W. A. *J. Acoust. Soc. Am.* **107,** 1286–1300 (2000).
3. Charif, R. A., Mellinger, D. K., Dunsmore, K. J., Fristrup, K. M. & Clark, C. W. *Mar. Mammal Sci.* **18,** 81–98 (2002).
4. Richardson, W. J., Greene, C. R., Malme, C. I. & Thomson, D. H. *Marine Mammals and Noise* (Academic, New York, 1995).
5. Schevill, W. E., Watkins, W. A. & Backus, R. H. in *Marine Bio-Acoustics* (ed. Tavolga, W. N.) 147–152 (Pergamon, New York, 1964).
6. Popper, A. N., Hawkins, H. L. & Gisiner, R. C. *Bioacoustics* **8,** 163–182 (1997).
7. Andrew, R. K., Howe, B. M. & Mercer, J. A. *Acoust. Res. Lett. Online* **3,** 65–70 (2002).
8. Watkins, W. A., Tyack, P., Moore, K. E. & Bird, J. E. *J. Acoust. Soc. Am.* **82,** 1901–1912 (1987).
9. Berube, M. & Palsboll, P. *Mol. Ecol.* **5,** 283–287 (1996).
10. Clapham, P. J. *Mammal Rev.* **26,** 27–49 (1996).
11. Croll, D. A., Acevedo-Gutierrez, A., Tershy, B. R. & Urban-Ramirez, J. *Comp. Biochem. Physiol. A* **129,** 797–809 (2001).
12. Clark, C. W. & Ellison, W. T. in *Echolocation in Bats and Dolphins* (eds Thomas, J., Moss, C. & Vater, M.) (Univ. Chicago Press, in the press).
13. Payne, R. S. & Webb, D. *Ann. NY Acad. Sci.* **188,** 110–141 (1971).

Competing financial interests: declared none.

Physiology

Dynamic instabilities in the inflating lung

In lung diseases such as asthma[1], expiratory flow becomes limited[2], airways can collapse[3] and the vital exchange of gases is compromised. Here we model the inflation of collapsed regions of the lung during inspiration in terms of avalanches propagating through a bifurcating network of airways, and find that the accompanying cascade of dynamic pressure instabilities — avalanche 'shocks' — manifests as negative elastic resistance of the lung. Our analysis of this apparent thermodynamic paradox provides a better understanding of aeration in the deep regions of the lung, which may find application in medical conditions in which gas exchange is impaired.

Most thermodynamic systems respond to an applied load by developing a restoring force — for example, when air is pumped into a rigid chamber, the pressure inside the chamber increases monotonically. However, during inflation of the mammalian lung from the collapsed state, the lung does not always develop an increasing restoring force; instead, the pressure inside the lung decreases intermittently. We explain this apparently paradoxical behaviour in terms

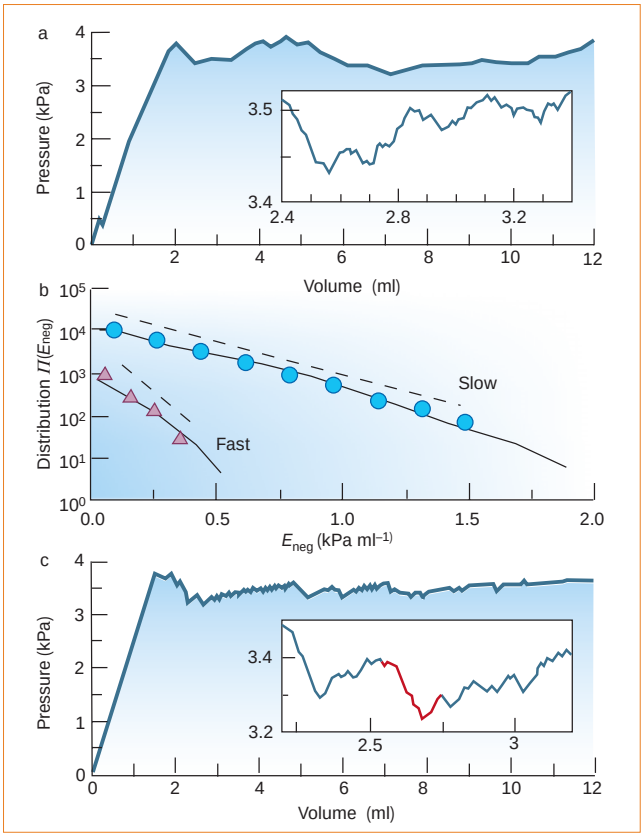

Figure 1 Pressure–volume curves and distributions of negative elastance. **a,** Example of the *P–V* curve (see text) during the inflation of a degassed rat lung. Inset, magnification of a region with many local negative-elastance patterns. **b,** Distributions of negative elastance from 10 independent inflations at rates of 2.0 ml s^{-1} (triangles) and 0.5 ml s^{-1} (circles). The values of E_0 obtained from the straight-line fits to the measured distributions are 0.28 kPa ml^{-1} and 0.1 kPa ml^{-1} for the slow and fast inflations, respectively (dashed lines). Solid lines correspond to the distributions of negative elastance from 1,000 simulated inflations of an 18-generation symmetric binary tree. **c,** Example of the *P–V* curve from inflation of the model. Inset, magnification of a region with many local negative-elastance patterns similar to those in **a**; red line, trace of an avalanche shock.

of a non-equilibrium avalanche model.

We inflated isolated, degassed rat lungs to total lung capacity at two different but constant rates by pumping in 12 ml of air with a computer-controlled piston. The lung recoil pressure, *P*, was then measured with respect to atmosphere as a function of the volume displacement, *V*, of the piston. With increasing *V*, *P* also increases, but this increase is not monotonic and *P* intermittently decreases (Fig. 1a), causing the elastance, *E* (defined as $E = dP/dV$), to take negative and positive values intermittently.

We estimate *E* as the local slope of a straight-line fit within a moving window along the *P–V* curve. The magnitude, E_{neg}, of elastances with negative values fluctuates. We find that the distribution $\Pi(E_{neg})$ is exponential,

$$\Pi(E_{neg}) \propto e^{-(E_{neg}/E_0)} \qquad (1)$$

where E_0, the characteristic value of E_{neg}, increases with inflation rate (Fig. 1b). The pattern of E_{neg} varies from inflation to inflation, but the distribution in equation (1) is reproducible. (This excludes the possibility that E_{neg} arises from tissue rupture.)

To understand the existence and fluctuations of the negative elastance, we developed a dynamical model of a system consisting of a piston chamber and a lung. We modelled the lung as a binary tree terminating in elastic alveoli[4]. The root of the tree, the trachea, is connected to the chamber containing 12 ml of air at atmospheric pressure, corresponding to the experimental conditions. Inflation is simulated by increasing *V* at a constant rate.

At the start of the inflation, all airways are closed and no alveoli are connected to the root, so a small increase in *V* increases *P*. A closed airway opens when *P* exceeds the airway's opening threshold pressure[5], P_{th}, which we assume to be a random variable uniformly distributed between 0 and 4 kilopascals (the pressure at total lung capacity). When a segment opens, the pressure propagates deeper into the airway tree. If the P_{th} of either daughter airway is also smaller than *P*, then this daughter opens together with its parent.

This process leads to an avalanche of openings involving a large number of airways and alveoli[6]. The newly opened airways and alveoli increase the volume of the lung, and *P* decreases according to Boyle's law. However, the reduction in *P* can terminate the propagation of the avalanche and *P* increases again owing to the steady influx of air — we term this phenomenon an avalanche shock (Fig. 1c, inset), which is not a conventional propagating shock wave.

The time course of an avalanche shock is smoothed by relaxation processes due to flow resistance in the airways[7] and the viscoelasticity of the alveolar walls[8]. The decreasing component of an avalanche shock corresponds to instabilities that are characterized by negative elastance. The continuous increase in *P* is intermittently interrupted by avalanche shocks of different magnitudes until all of the air in the chamber is injected into the lung.

The model produces *P–V* curves (Fig. 1c) that are similar to those observed experimentally (Fig. 1a). The local E_{neg} is determined in the same way as for the measured data. The distributions $\Pi(E_{neg})$ from the simulations fit the experimentally obtained distributions for both slow and fast inflation rates (Fig. 1b). These results indicate that inflating the lung from a state in which a considerable part of the gas-exchange region is collapsed is a non-equilibrium dynamical process characterized by a sequence of instabilities with negative elastance.

For slow inflation, the system has enough time after each avalanche to reach equilibrium, so the individual avalanche shocks are distinct and non-overlapping. With increasing inflation rate, however, avalanche shocks due to separate avalanches increasingly overlap, resulting in smoother *P–V* curves with fewer regions of negative elastance. We conclude that the paradoxical negative elastance and its distribution arise from avalanche shocks involving the sudden recruitment and subsequent relaxation of a large number of airways and alveoli.

Instabilities related to airway and alveolar collapse and recruitment have a key function in impaired gas exchange in premature infants[9], in sufferers of severe asthma[3] or after acute lung injury[10]. These instabilities have previously been attributed to a combination of the static properties of the alveolar liquid lining[11] and the non-uniform deformation of lung tissue[12]. Our results and quantitative modelling provide a new interpretation of these instabilities.

Adriano M. Alencar*†, Stephen P. Arold*, Sergey V. Buldyrev†, Arnab Majumdar†, Dimitrije Stamenović*, H. Eugene Stanley†, Béla Suki*

**Department of Biomedical Engineering, and †Center for Polymer Studies and Department of Physics, Boston University, Boston, Massachusetts 02215, USA*
e-mail: adriano@bu.edu

1. Tobin, M. J. *Am. J. Crit. Care Med.* **165,** 598–618 (2002).
2. Mead, J., Turner, J. M., Macklem, P. T. & Little, J. B. *J. Appl. Physiol.* **22,** 95–108 (1967).
3. Lutchen, K. R., Kaczka, D. W., Israel, E., Suki, B. & Ingenito, E. P. *Am. J. Crit. Care Med.* **164,** 207–215 (2001).
4. Shlesinger, M. F. & West, B. J. *Phys. Rev. Lett.* **67,** 2106–2108 (1991).
5. Gaver, D. P., Samsel, R. W. & Solway, J. *J. Appl. Physiol.* **69,** 74–85 (1990).
6. Suki, B. *et al. Nature* **368,** 615–618 (1994).
7. Pedley, T. J., Schroter, R. C. & Sudlow, M. F. *Respir. Physiol.* **9,** 387–405 (1970).
8. Fukaya, H., Martin, C. J., Young, A. C. & Katsura, S. *J. Appl. Physiol.* **25,** 689–695 (1968).
9. Pattle, R. E., Claireaux, A. E., Davis, P. A. & Cameron, A. H. *Lancet* **2,** 469–473 (1962).
10. Muscedere, J. G., Mullen, J. B., Gan, K. & Slutsky, A. S.

Am. J. Crit. Care Med. **149,** 1327–1334 (1994).
11. Clements, J. A., Hustead, R. F., Johnson, R. T. & Gribetz, I. *J. Appl. Physiol.* **16,** 444–450 (1961).
12. Stamenovic, D. & Wilson, T. A. *J. Appl. Physiol.* **73,** 596–602 (1992).
Competing financial interests: declared none.

Surface phenomena

Contact time of a bouncing drop

When a liquid drop lands on a solid surface without wetting it, it bounces with remarkable elasticity[1–3]. Here we measure how long the drop remains in contact with the solid during the shock, a problem that was considered by Hertz[4] for a bouncing ball. Our findings could help to quantify the efficiency of water-repellent surfaces (super-hydrophobic solids[5]) and to improve water-cooling of hot solids, which is limited by the rebounding of drops[6] as well as by temperature effects.

The way in which a water drop of radius R deforms during its impact with a highly hydrophobic solid depends mainly on its impinging velocity, V. The Weber number, $W=\rho V^2R/\gamma$, compares the kinetic and surface energies of the drop, where ρ and γ are the liquid density and surface tension, respectively. The greater the value of W, the larger are the deformations that occur during the impact (Fig. 1).

High-speed photography (Fig. 1) enabled us to measure the drop's contact time, τ. The frame rate could be greater than 10^4 Hz, allowing precise measurements of τ, which we found to be in the range 1–10 ms. As the impact is mainly inertial (with a restitution coefficient[2] as great as 0.91), τ is expected to be a function of only R, V, ρ and γ, and thus to vary as $R/V.f(W)$. For a Hertz shock, for example, the maximum vertical deformation, δ, scales as $R(\rho^2V^4/E^2)^{1/5}$, where E is the Young's modulus of the ball[7]. Taking a drop's Laplace pressure, $E\approx\gamma/R$, as an equivalent modulus and noting that $\tau\approx\delta/V$, we find for a Hertz drop that $f(W)\sim W^{2/5}$ and that the contact time varies as $V^{-1/5}$ and $R^{7/5}$.

Figure 2a shows that the contact time does not depend on the impact velocity over a wide range of velocities (20–230 cm s^{-1}), although both the deformation amplitude and the details of the intermediate stages largely depend on it. This is similar to the case of a harmonic spring, although oscillations in the drop are far from being linear. Moreover, this finding confirms that viscosity is not important here.

Figure 2b shows that τ is mainly fixed by the drop radius, because it is well fitted by $R^{3/2}$ over a wide range of radii (0.1–4.0 mm). Both this result and the finding shown in Fig. 2a can be understood simply by balancing inertia (of the order $\rho R/\tau^2$) with capillarity (γ/R^2), which yields $\tau\approx(\rho R^3/\gamma)^{1/2}$, of the form already stated with $f(W)\sim W^{1/2}$. This time is slightly different from the Hertz time because the kinetic energy for a solid is stored during the impact in a localized region, whereas in our case it forces an overall deformation of the drop (Fig. 1).

The scaling for τ is the same as for the period of vibration of a drop derived by Rayleigh[8], and is consistent with a previous postulation[9], although the motion here is asymmetric in time, forced against a solid, and of very large amplitude. Absolute values are indeed found to be different: the prefactor deduced from Fig. 2b is 2.6 ± 0.1, which is significantly greater than $\pi/\sqrt{2}\approx2.2$ for an oscillating drop[8]. Another difference between the two systems is the behaviour in the linear regime ($W\ll1$): for speeds less than those shown in Fig. 2, we found that τ depends on V, and typically doubles when V is reduced from 20 to 5 cm s^{-1}, which could be due to the drop's weight[10].

The brevity of the contact means that a drop that contains surfactants, which will spread when gently deposited onto the solid, can bounce when thrown onto it; this is because the contact time is too short to allow the adsorption of the surfactants onto the fresh interface generated by the shock. Conversely, the contact time should provide a measurement of the dynamic surface tension of the drop.

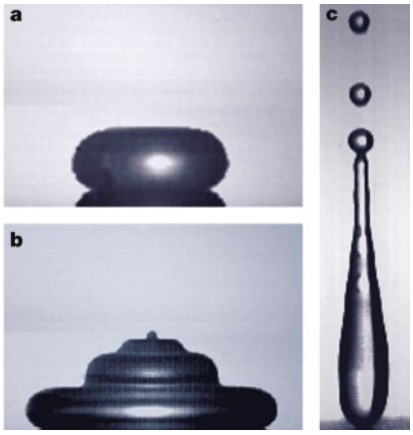

Figure 1 Millimetre-sized water drops with different Weber numbers (W) hitting a super-hydrophobic solid. W compares the kinetic and surface energies of the drop ($W=\rho V^2R/\gamma$, where R is the drop radius, V is the impact velocity, and ρ and γ are the density and surface tension, respectively, of the liquid). **a,** When W is close to unity, the maximum deformation during contact becomes significant. **b,** When $W\approx4$, waves develop along the surface and structure the drop. **c,** When $W\approx18$, the drop becomes highly elongated before detaching and gives rise to droplets; however, the contact time is independent of the details of the impact (see Fig. 2a).

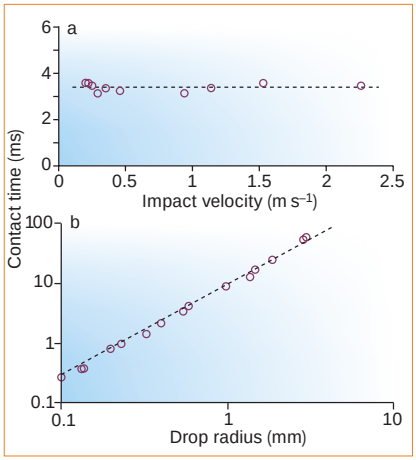

Figure 2 Contact time of a bouncing drop as a function of impact velocity and drop radius. **a, b,** In the explored interval (Weber number, W, between 0.3 and 37), the contact time is **a**, independent of the impact velocity, V, but **b**, depends on the drop radius, R. Dotted lines indicate slopes of 0 (**a**) and 3/2 (**b**).

Denis Richard*, Christophe Clanet†, David Quéré*
**Laboratoire de Physique de la Matière Condensée, URA 792 du CNRS, Collège de France, 75231 Paris Cedex 05, France*
e-mail: quere@ext.jussieu.fr
†Institut de Recherche sur les Phénomènes Hors Équilibre, UMR 6594 du CNRS, BP 146, 13384 Marseille Cedex, France

1. Hartley, G. S. & Brunskill, R. T. in *Surface Phenomena in Chemistry and Biology* (ed. Danielli, J. F.) 214 (Pergamon, Oxford, 1958).
2. Richard, D. & Quéré, D. *Europhys. Lett.* **50,** 769–775 (2000).
3. Aussillous, P. & Quéré, D. *Nature* **411,** 924–927 (2001).
4. Hertz, H. *J. Reine Angew. Math.* **92,** 156–171 (1881).
5. Nakajima, A., Hashimoto, K. & Watanabe, T. *Monatshefte Chim.* **132,** 31–41 (2001).
6. Frohn, A. & Roth, R. *Dynamics of Droplets* (Springer, Berlin, 2000).
7. Landau, L. D. & Lifschitz, E. M. *Theory of Elasticity* 3rd edn (Pergamon, Oxford, 1986).
8. Rayleigh, Lord *Proc. R. Soc. Lond. A* **29,** 71–97 (1879).
9. Wachters, L. H. J. & Westerling, N. A. J. *Chem. Eng. Sci.* **21,** 1047–1056 (1966).
10. Perez, M. *et al. Europhys Lett.* **47,** 189–195 (1999).
Competing financial interests: declared none.

Evolutionary biology

Hedgehog crosses the snail's midline

According to the dorsoventral axis-inversion theory[1], protostomes (such as insects, snails and worms) are organized upside-down by comparison with deuterostomes (vertebrates)[2–5], in which case their respective ventrally (belly-side) and dorsally (back-side) located nervous systems, as well as their midline regions, should all be derived from a common ancestor[5]. Here we provide experimental evidence for such homology by showing that an orthologue of *hedgehog*, an important gene in midline patterning in vertebrates, is expressed along the belly of the larva of the limpet *Patella vulgata*. This